



Kent Academic Repository

Wozniakiewicz, Penelope J., Kearsley, Anton T., Burchell, Mark J., Price, Mark C., Ishii, Hope A. and Cole, Michael J. (2018) *Preparation of large Stardust aluminum foil craters for analysis*. *Meteoritics and Planetary Science*, 53 (5). pp. 1066-1080. ISSN 1086-9379.

Downloaded from

<https://kar.kent.ac.uk/66427/> The University of Kent's Academic Repository KAR

The version of record is available from

<https://doi.org/10.1111/maps.13052?>

This document version

Publisher pdf

DOI for this version

Licence for this version

CC BY (Attribution)

Additional information

Versions of research works

Versions of Record

If this version is the version of record, it is the same as the published version available on the publisher's web site. Cite as the published version.

Author Accepted Manuscripts

If this document is identified as the Author Accepted Manuscript it is the version after peer review but before type setting, copy editing or publisher branding. Cite as Surname, Initial. (Year) 'Title of article'. To be published in *Title of Journal*, Volume and issue numbers [peer-reviewed accepted version]. Available at: DOI or URL (Accessed: date).

Enquiries

If you have questions about this document contact ResearchSupport@kent.ac.uk. Please include the URL of the record in KAR. If you believe that your, or a third party's rights have been compromised through this document please see our [Take Down policy](https://www.kent.ac.uk/guides/kar-the-kent-academic-repository#policies) (available from <https://www.kent.ac.uk/guides/kar-the-kent-academic-repository#policies>).

Preparation of large Stardust aluminum foil craters for analysis

Penelope J. WOZNIAKIEWICZ^{1,2,*}, Anton T. KEARSLEY^{3,4}, Mark J. BURCHELL¹,
Mark C. PRICE¹, Hope A. ISHII⁵, and Michael J. COLE¹

¹School of Physical Science, University of Kent, Canterbury CT2 7NH, UK

²Department of Earth Sciences, Natural History Museum, London SW7 5BD, UK

³Dunholme, Raven Hall Road, Ravenscar, North Yorkshire YO13 0NA, UK

⁴Imaging and Analysis Centre, Natural History Museum, London SW7 5BD, UK

⁵Hawai'i Institute of Geophysics and Planetology, University of Hawai'i at Manoa, 1680 East-West Road, POST 602,
Honolulu, Hawai'i 96822, USA

*Corresponding author. E-mail: pjw@kent.ac.uk

(Received 28 November 2017; revision accepted 10 January 2018)

Abstract—Over the last decade, silica aerogel tracks and aluminum foil craters on the Stardust collector have been studied extensively to determine the nature of captured cometary dust grains. Analysis of particles captured in aerogel has been developed to a fine art, aided by sophisticated preparation techniques, and yielding revolutionary knowledge of comet dust mineralogy. The Stardust foil craters can be interpreted in terms of impacting particle size and structure, but almost all studies of composition for their contents have relied on in situ analysis techniques or relatively destructive extraction of materials. This has limited their examination and interpretation. However, numerous experimental hypervelocity impact studies under Stardust-Wild 2 encounter conditions have shown that abundant dust components are preserved in foil craters of all sizes. Using some of these analogue materials, we have previously shown that modern, nondestructive scanning electron microscope imaging and X-ray microanalysis techniques can document distribution of dust remnants both quickly and thoroughly within foil craters prior to any preparation. Here we present findings from our efforts to quantify the amount of residue and demonstrate a simple method of crater shape modification which can bring material into positions where it is much more accessible for in situ analysis, or safe removal of small subsamples. We report that approximately 50% of silicate-dominated impactors were retained as impact crater residue; however, <3% of organic impactors remained in the craters after impact.

INTRODUCTION

The Stardust mission to comet Wild 2 returned samples of captured dust (Brownlee et al. 2006) that probably total <1 mg in weight. Despite this very small mass, the materials analyzed in the first decade of research since sample return have revolutionized our understanding of comet composition and early solar system processes. The majority of analytical work thus far, especially mineralogy and petrology (e.g., Nakamura et al. 2008; Zolensky et al. 2008), has been

performed on grains captured in the primary collection medium, density-graded silica aerogel. The development of the “keystone” extraction technique by Westphal et al. (2004), the “quickstone” extraction technique by Ishii et al. (2005), Ishii and Bradley (2006), and the widespread use of in situ synchrotron analysis and imaging (e.g., Flynn et al. 2006; Tsuchiyama et al. 2009), epoxy mounting and ultramicrotome sectioning followed by analytical transmission electron microscopy (TEM; e.g., Stodolna et al. 2009; Nakamura-Messenger et al. 2011) have been very successful. The relative

“transparency” of the low-density medium to electromagnetic radiation of optical, infrared, and X-ray wavelengths has allowed a wide range of techniques (e.g., Ebel et al. 2009) to be employed in finding locations for extraction of specific grains. Unfortunately, small dust grains and some finer grained components of larger aggregates may undergo significant processing by interaction with hot, compressed silica during their capture in aerogel (e.g., Leroux et al. 2008a; Ishii and Bradley 2015). This may complicate determination of composition (especially the original oxygen isotope ratios of the impactor), and has encouraged a few authors to pursue isotopic analysis in Stardust Al alloy foil craters (e.g., Snead et al. 2014, 2017).

The numerous craters on the Stardust aluminum 1100 foils show impacts by Wild 2 dust grains of a wide size range (Hörz et al. 2006). Extensive testing of sample preparation and microanalysis techniques, such as focused ion beam (FIB) sectioning (e.g., Graham et al. 2006) and Raman spectroscopy (e.g., Burchell et al. 2008), using analogue materials produced by hypervelocity impact experiments prior to the return of the Stardust capsule, enabled evaluation of appropriate methods. During the preliminary examination (PE) of the cometary dust collector, foil craters were surveyed using scanning electron microscopy (SEM) with energy-dispersive X-ray (EDX) microanalysis to ascertain crater dimensions and approximate residue chemistry (e.g., Kearsley et al. 2008). Some smaller (micrometer-scale) craters were also analyzed by preparing sections across entire craters using FIB (e.g., Leroux et al. 2008b) for study of their residues by TEM. However, there has since been relatively little further study of the contents of larger craters (>20 μm diameter) beyond PE. Partly, this has been due to the expectation that high peak pressures during foil impact, estimated to be between 60 and 90 GPa depending on the impactor composition (Burchell and Kearsley 2009), would result in vaporization and loss of much of the impactor. In the first part of this paper, we demonstrate that a substantial quantity may remain by using three methods to locate and measure the proportion of the particle that is retained within calibrated experimental analogue craters created under Stardust capture conditions.

Regarding the state of impactor preservation, TEM analyses of smaller Stardust craters have already shown significant preservation of crystalline material (e.g., Leroux et al. 2008b), and comparison of the crater dimensions to the calibration of Price et al. (2010) suggests that a large proportion of the impacting grain was retained. Although extensive TEM studies of larger Stardust craters have not been performed, laser Raman spectra of their residues (Foster et al. 2013) also show

that some structural mineral information does clearly survive. Light-gas gun (LGG) experimental impacts of a wide range of minerals have now produced analogue samples, in which FIB-prepared sections show abundant impactor residue, including preserved crystalline material (Wozniakiewicz et al. 2009, 2011, 2012a, 2012b, 2015). Together, these results suggest that there is much, albeit as yet unrealized, promise in larger Stardust craters—if a suitable method for location and extraction of subsamples were available.

Relatively small ultra-thin sections were successfully extracted from smaller Stardust craters by filling the crater with platinum, and subsequently FIB milling to release a section showing the whole crater width, including dust remains for further analysis by TEM (Leroux et al. 2008b). However, as FIB sections of >10 μm length have a tendency to warp and are very difficult to handle without damage, this preparation process is not suitable for craters larger than \sim 10 μm diameter. The topography of larger impact craters has also proven difficult for removal of FIB sections as the extraction angle is usually too steep for an in-chamber micromanipulator to reach cut sections. Attempts to extract FIB sections directly from such large impact craters are therefore restricted to accessing material within reach of micromanipulators, high on crater walls and rims where the residue is often less abundant (e.g., Graham et al. 2006). There has also been understandable reluctance to attempt extraction of smaller samples by FIB from deep within intact larger Stardust craters (up to >300 μm), as the size and shape of these larger craters is likely to generate widespread and highly undesirable surface contamination, by redeposition of FIB-ablated material. To enable TEM studies of mineral preservation in large Stardust analogue craters, FIB access to the abundant residues lining crater floors has been facilitated by either flattening crater rims (Wozniakiewicz et al. 2012b) or embedding foils in epoxy resin and mechanically polishing down until a suitable crater cross section was exposed (Wozniakiewicz et al. 2011, 2012b, 2015). Although very effective, this method necessarily destroys much of the crater, and would not be appropriate for the precious Stardust samples.

Before attempting any extraction of subsamples for analysis, it is obviously also important to know where the residue is present, and what it may be. Detailed mapping of residue location to obtain information from throughout the deep profile of larger bowl-shaped craters presents a substantial problem for conventional SEM EDX (e.g., Kearsley et al. 2007). For most ion beam instruments, this lack of preliminary mapping information detailing the diversity and spatial distribution of crater contents prior to isotopic analysis

could also result in undesirable simultaneous collection of data from more than one dust component. Together, these problems have given pause to use of FIB along with other preparation and analysis techniques on large crater dust residues.

Auger electron mapping has been applied successfully to give elemental maps throughout the depth of Stardust craters (Stadermann and Floss 2008), but this technique is slow to document large areas. Fortunately, the most modern EDX detectors based on very clean SEM instruments (e.g., Wozniakiewicz et al. 2015), can find residue not only on the walls and lips of craters (which may be good targets for in situ isotopic microanalysis by instruments such as NanoSIMS, e.g., Stadermann et al. 2008) but also reveal material even in the deeper parts, not seen by conventional inclined EDX detectors. Now that the distribution of dust remnants throughout a crater can be determined, if there were a simple and reliable technique to change crater shapes for safe extraction of said material, there would be an opportunity to make much more use of the large foil craters. For example, to enable SIMS analyses, Snead (2016) cut individual craters free from the surrounding foil, and flattened them mechanically between glass slides. In the second part of this paper, we describe laboratory experiments and an alternative, simple mechanical method that allowed us to modify crater profiles, making them flatter for better surface access. Such improvements are in line with the call in Westphal et al. (2017) for greater use of analogue samples and better laboratory techniques to enable the second decade of Stardust science. For example, 63 craters of $>20\ \mu\text{m}$ diameter were identified during PE, and although several have subsequently been consumed for SIMS measurements, many remain unexamined and potentially valuable for future study—researchers may wish to contact the Stardust curator to enquire about their availability.

METHODS

Calibrated Analogue Impacts to Measure Extent of Particle Retention

For our investigations into the extent of impacting particle retention within crater residues, four types of material were prepared as sabot-mounted buckshot powders for experimental impact onto Stardust Al 1100 foil by two-stage LGG (Burchell et al. 1999) at the University of Kent in Canterbury:

- a) Monodisperse soda-lime glass spheres of $11.58\ \mu\text{m}$ diameter (shots G120509#1 at $1.13\ \text{km s}^{-1}$ and G030608#2 at $1.92\ \text{km s}^{-1}$) and $22.8\ \mu\text{m}$ diameter (shots G120509#2 at $2.93\ \text{km s}^{-1}$, G180509#1 at $4.43\ \text{km s}^{-1}$, G100809#1 at $6.05\ \text{km s}^{-1}$, G050509#2 at $6.48\ \text{km s}^{-1}$, and G050509#3 at $7.65\ \text{km s}^{-1}$). Secondary electron images (SEI) at high beam energy (20 keV), and stereo pair backscattered electron images (BEI) of the resulting craters were collected in the Zeiss EVO 15 LS SEM at the Natural History Museum (NHM) London. Digital elevation models (DEM) and depth profiles were created using Alicona MeX 4.2 software.
- b) Monodisperse silica spheres of $\sim 1.6\ \mu\text{m}$ diameter (shot G060509#1 at $6.27\ \text{km s}^{-1}$). A typical foil crater was imaged in the FEI Nova Nanolab 600 dual beam FIB at FEI NanoPort (Hillsboro, Oregon, USA), and filled with electron beam-deposited platinum. Precisely measured FIB milling generated 23 sequential vertical cut surfaces for which SEI were obtained and used to measure crater and residue dimensions.
- c) Powdered silicate glass, organic, diverse mineral and meteorite samples, including: NKT-1G standard basalt glass; polyoxymethylene, urea, olivine from the Admire pallasite meteorite; diopside clinopyroxene; enstatite orthopyroxene; bytownite feldspar; lizardite serpentine; cronstedtite; calcite; pentlandite; kamacite; mineral aggregates; carbonaceous chondrite meteorites Allende (CV3) and Orgueil (CI); eucrite meteorite NWA 1895; and the ordinary chondrite meteorite Bjurböle. All were shot at a velocity of $\sim 6\ \text{km s}^{-1}$. SEI were acquired at low beam energy (2 keV) to show the location and hence extent of residue. Additional BEI at high energy (20 keV) was performed to reveal characteristic surface textures within the craters. One crater from shot G180808#1 (Bjurböle, at $6.24\ \text{km s}^{-1}$) was imaged, measured, and analyzed in detail by BEI and inclined EDX in the Zeiss EVO 15LS SEM at the NHM. A DEM was created from stereo BEI to quantify crater surface area. EDX elemental maps were acquired from four rotation positions, yielding data from all except a very small area of the crater floor, giving quantified surface area coverage. By assuming an average residue thickness based on our previous observations of residues in cross section, an estimate of residue volume was made.
- d) Organic polymers for measurement of remaining carbon: polymethylmethacrylate (PMMA) of $30\ \mu\text{m}$ diameter (shot G090506#1 at $5.97\ \text{km s}^{-1}$) and polystyrene (PST) of $40\ \mu\text{m}$ diameter (shot G180209#3 at $6.10\ \text{km s}^{-1}$). The Oxford Instruments INCA EDX on the Zeiss EVO 15 LS SEM at NHM was calibrated for carbon film thickness measurement using the protocol described in Stroud et al. (2014). SEM EDX spectra were collected from areas of the

distinctive crater floor textures, and were compared to the carbon film thickness calibration curve. DEM were created from stereo BEI to quantify crater surface areas, to calculate the total volume of the carbon-bearing residue.

Analogue Impact Craters for Testing Foil Preparation Methods

A small sample of natural galena (lead sulfide, PbS) was powdered as projectile material. Galena was chosen as it has a relatively high mean atomic number and therefore produces a residue with high backscatter coefficient, easily visible in the detailed stereo images of craters necessary for three-dimensional shape reconstruction in this test program. The impactor density was also sufficient to produce craters of a depth comparable with deeper (worst case) Stardust craters. The powder was fired onto a 100 μm thick Al 1100 foil at $\sim 6 \text{ km s}^{-1}$ (shot G241109#2 at 6.14 km s^{-1}).

A strip of the impacted foil, similar in size to those cut from the Stardust collector, was carefully laid across the aperture of a butterfly hinge (Fig. 1a), so that the craters to be prepared were visible through the central hole. The hinge was closed and bolted together, holding the foil gently but securely for initial examination in the SEM, and for subsequent preparation. BEI, with carefully registered image pairs acquired at 6 degree angular separation, was performed on the Zeiss EVO 15LS at the NHM. DEM were created for the craters before preparation, and after deformation of the foil. A steel needle, with the tip modified to produce a broad, rounded dome profile, was mounted within a cylindrical resin block (Fig. 1b). Initial SEM imaging was followed by modification of the crater shape, with the hinge held carefully between fingers and slowly lowered down onto the tip of the needle (Fig. 1c), while the crater was observed through a binocular microscope. After the area of the crater floor had been pushed up to the level of the surrounding foil (or above), the hinge and contained craters were again imaged in the SEM (Fig. 1d).

RESULTS

Retention of Impacting Particle Residue

a) SEI taken at high electron beam energy (20 keV) show a progressive change in the style of glass impactor retention as a function of impact velocity (Fig. 2). In Table 1 we give the peak shock pressure associated with the impact speeds of the examples in Fig. 2. These were found using the planar impact approximation (Melosh 1989). At the lowest impact velocity, the spherical glass bead (e.g., Fig. 2a) has

created a bowl-shaped crater of the same diameter as the projectile (Fig. 2b), but has rebounded, leaving no visible remains. We also note the absence of a broad overturned crater rim commonly observed on (higher velocity) Stardust craters. At velocities between ~ 2 and 3 km s^{-1} (Figs. 2c and 2d) the projectile is retained, but with substantial fracturing visible at the rear, increasing with velocity. Above $\sim 4 \text{ km s}^{-1}$ (Fig. 2e) the structure of the glass bead breaks down, leaving small angular fragments protruding from a sheet of frozen melt. At a velocity greater than 6 km s^{-1} (Figs. 2f–h) a bowl-shaped crater is developed with a lining of frozen glass melt. As impact velocity increases, we observe an increase in the extent of glass impactor deformation and melting.

- b) The SEI of FIB cut surfaces through the small crater reveal retention of residue in a layer of $\sim 90 \text{ nm}$ thickness (Fig. 3, bottom), covering $\sim 50\%$ of the near-hemispherical internal surface. Residue can be traced through successive images (Fig. 3, top). The impacting silica sphere diameter ($1.6 \mu\text{m}$) was determined by comparison of the crater maximum internal diameter at the preimpact plane ($3.63 \mu\text{m}$) to the calibration of Price et al. (2010). Assuming a spherical particle shape (as seen in SEM images of the projectiles before firing), this gives a volume of $2.24 \mu\text{m}^3$. Integrating the visible residue areas and thickness throughout the crater slices gives a volume of $\sim 0.89 \mu\text{m}^3$, equivalent to $\sim 40\%$ of the original projectile. This is consistent with observations in Leroux et al. (2008b), where, if their data for $\sim \mu\text{m}$ -sized Stardust craters are corrected using the updated projectile to crater diameter relations reported in Price et al. (2010), craters appear to have retained between $\sim 20\%$ and 80% of the original impactor.
- c) Distribution of residue within craters was revealed by the darker gray tones in the SEI (Fig. 4), due to relatively shallow beam penetration and poor secondary emission from the electrically insulating residue, compared to the alloy foil substrate. These images show that the residue is widespread at depth within the craters, as also revealed by the novel EDX detector maps of Wozniakiewicz et al. (2015). Surface textures seen in BEI (Fig. 5) also reveal both the location and some information about the behavior of the projectile material. Basalt glass produces a smooth crater lining (like soda-lime glass in Fig. 2f), whereas crystalline anhydrous silicates such as diopside retain angular fragments (as also seen for olivine impacts by Wozniakiewicz et al. 2015). Hydrous silicate aggregates (such as lizardite) and artificial polymer-cemented mineral

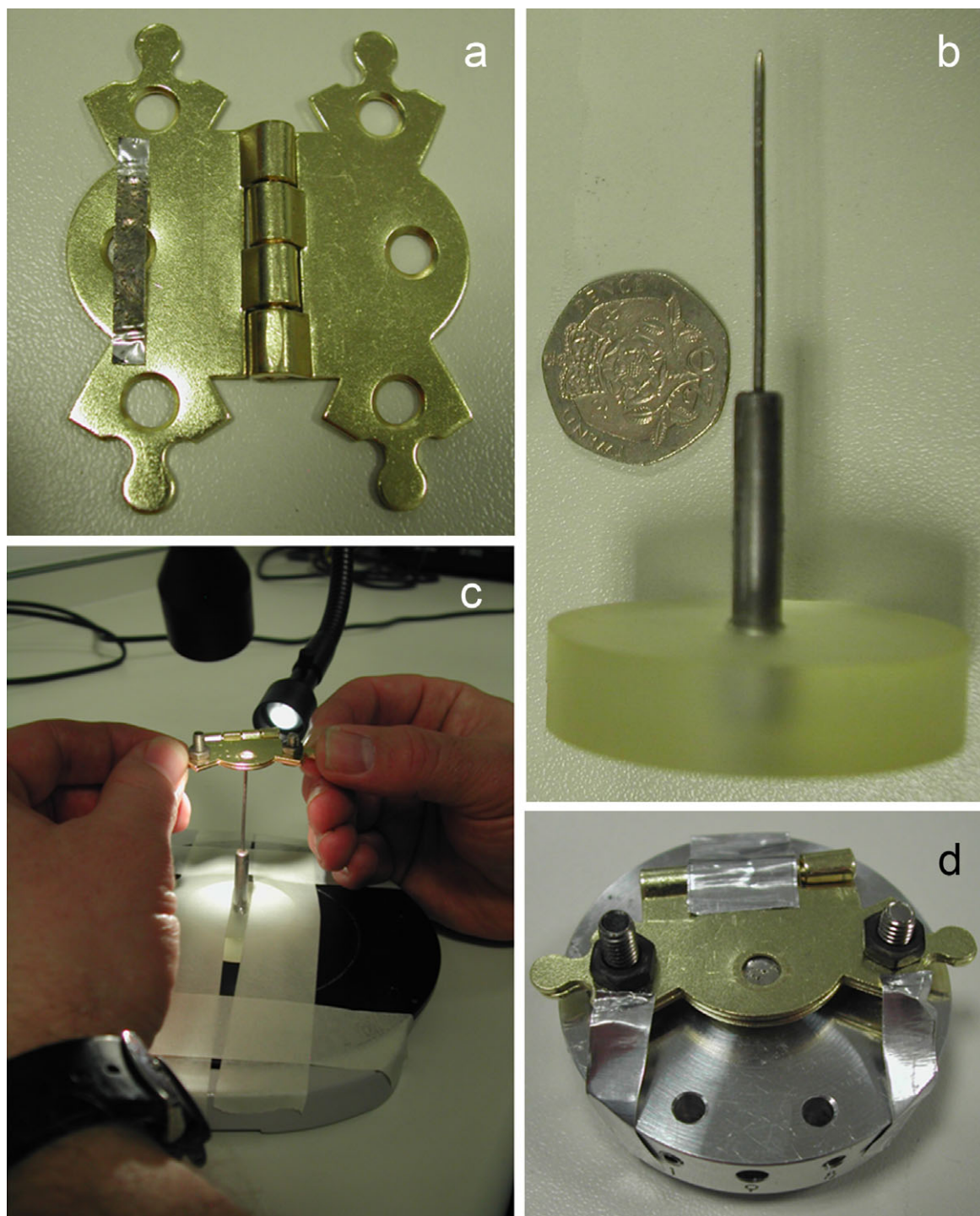


Fig. 1. a) An impacted foil strip laid across the butterfly hinge, ready for clamping. b) The tool used for modification of crater shape. c) The foil held within the hinge is carefully pushed down onto the rounded needle tip, while observed through the stereo binocular microscope. d) An impacted foil, held within the closed butterfly hinge, mounted on the SEM sample holder for imaging.

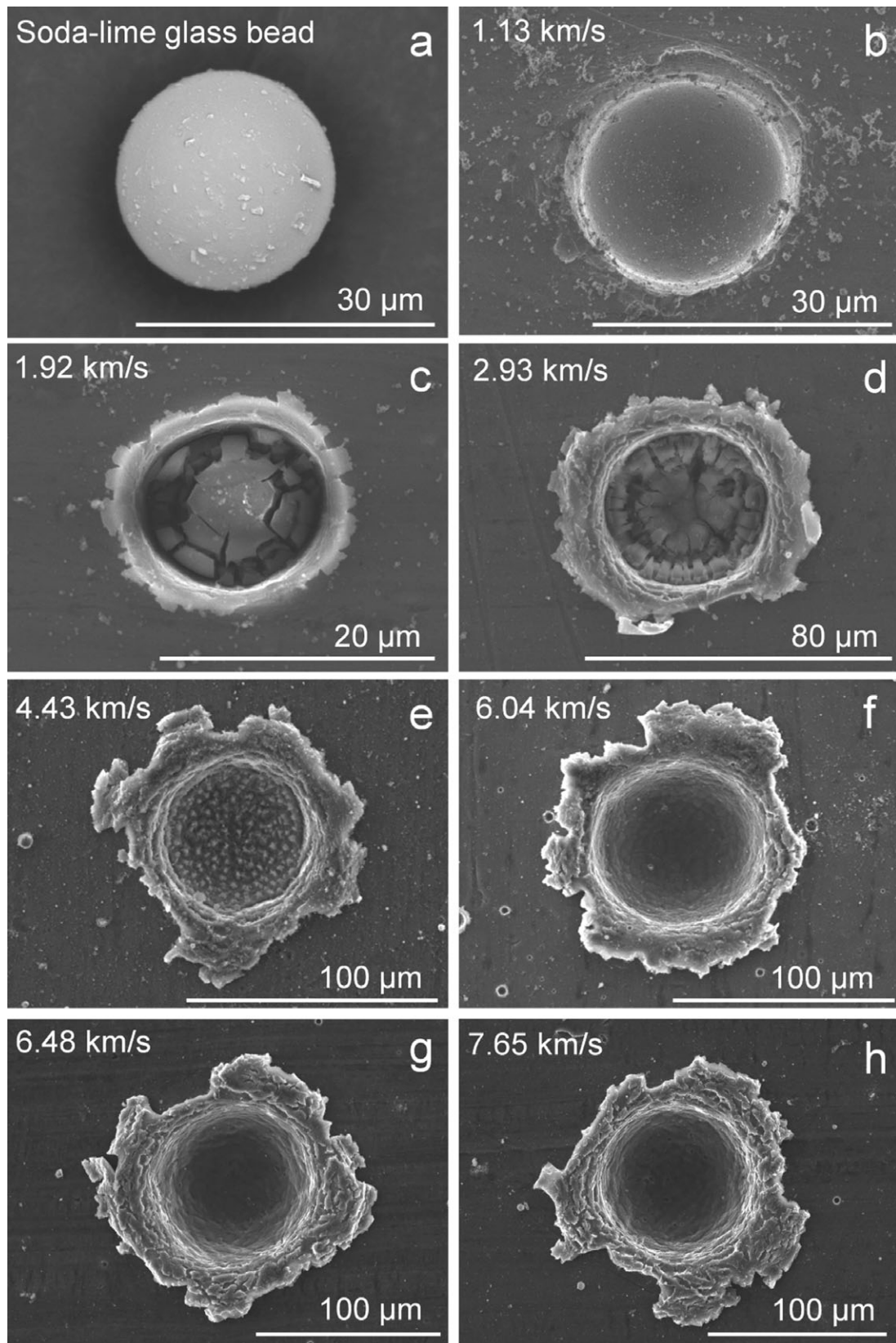


Fig. 2. SEM images of (a) typical soda-lime glass projectile; (b–h) LGG shot craters produced by impact of soda-lime glass spheres onto Stardust Al 1100 foil at varying velocity.

Table 1. Peak shock pressures in aluminum 1100 targets impacted by soda-lime glass. Pressures were calculated using Planar Impact Approximation (see main text for details). This requires a linear shock-particle velocity equation of state wherein $U_s = C + Su_p$. For aluminum, we use $C = 5.332$, $S = 1.375$, and a density of 2750 kg m^{-3} (Marsh 1980), and for the soda-lime glass we use $C = 0.14$, $S = 1.92$, and density 2520 kg m^{-3} (Kobayashi et al. 1998).

Impact speed (km s^{-1})	Pressure (GPa)
1.13	4.01
1.92	9.43
2.93	18.6
4.43	36.5
6.05	61.4
6.48	68.9
7.65	91.4

aggregates leave irregular, twisted, ropy surfaces, possibly reflecting interference between expanding excavation fields driven by synchronous impacts of laterally separated subgrains. Although Stardust craters of such multimaterial impacts have been found to contain remnant crystalline grains, it may be that surviving crystals only occur where the impacting grain is just a few times the size of its components grains. Those residues of large Stardust analogue aggregates composed of much finer subgrains instead exhibit complete melting and no retention of micrometer-scale angular fragments (Wozniakiewicz et al. 2012a). Relatively dense sulfides (such as pentlandite) and metals (such as kamacite) leave frozen droplets and pools of immiscible residue. Organic impactors create a very distinctive texture of polygonal fractures in the crater lining, possibly the result of rapid quenching and contraction of melt, due to surface chilling by evaporation of organic residue. Those volatile-bearing impactors (e.g., water-bearing lizardite, sulfur-bearing pyrrhotite, and pentlandite) also exhibit vesiculated textures in some regions, resulting from the loss of volatiles during impact (Wozniakiewicz et al. 2015).

The measured top-lip diameter of the Bjurböle impact crater from shot G180808#1 was $439.7 \mu\text{m}$. Based on the comparison to the soda-lime glass calibration of Kearsley et al. (2007), this would suggest an impacting grain of $\sim 95 \mu\text{m}$ diameter, with an assumed spherical volume of $\sim 448,472 \mu\text{m}^3$. The area of residue on the crater surface in the calibrated DEM was $\sim 125,377 \mu\text{m}^2$ (Fig. 6). Similar morphology craters sectioned by FIB (e.g., basalt glass craters in Kearsley et al. [2007]; olivine,

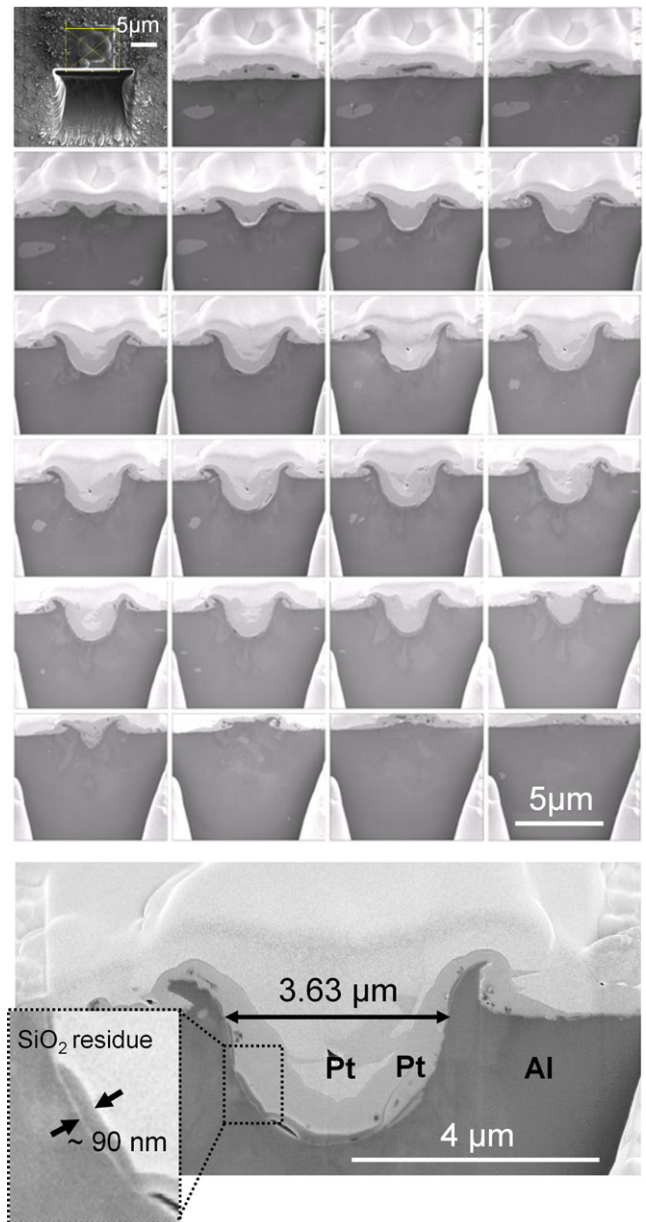


Fig. 3. Electron-stimulated SEI in the FIB SEM showing (top left) FIB trench at the beginning of crater cutting, and oblique images of sequential cuts through the entire crater, rescaled to give correct crater depth profile (bottom) section at maximum diameter of crater formed by silica sphere impact with Al and both electron- and ion-beam-deposited Pt layers labeled; inset shows residue layer thickness.

diopside, pyrrhotite, pentlandite, and fine-grained aggregate craters in Wozniakiewicz et al. [2012a]; and calcite, cronstedtite, and lizardite craters in Wozniakiewicz et al. [2015]) show an average of $2 \mu\text{m}$ thickness of residue, suggesting a total volume of $\sim 250,754 \mu\text{m}^3$ in this crater, $\sim 56\%$ of the original particle volume.

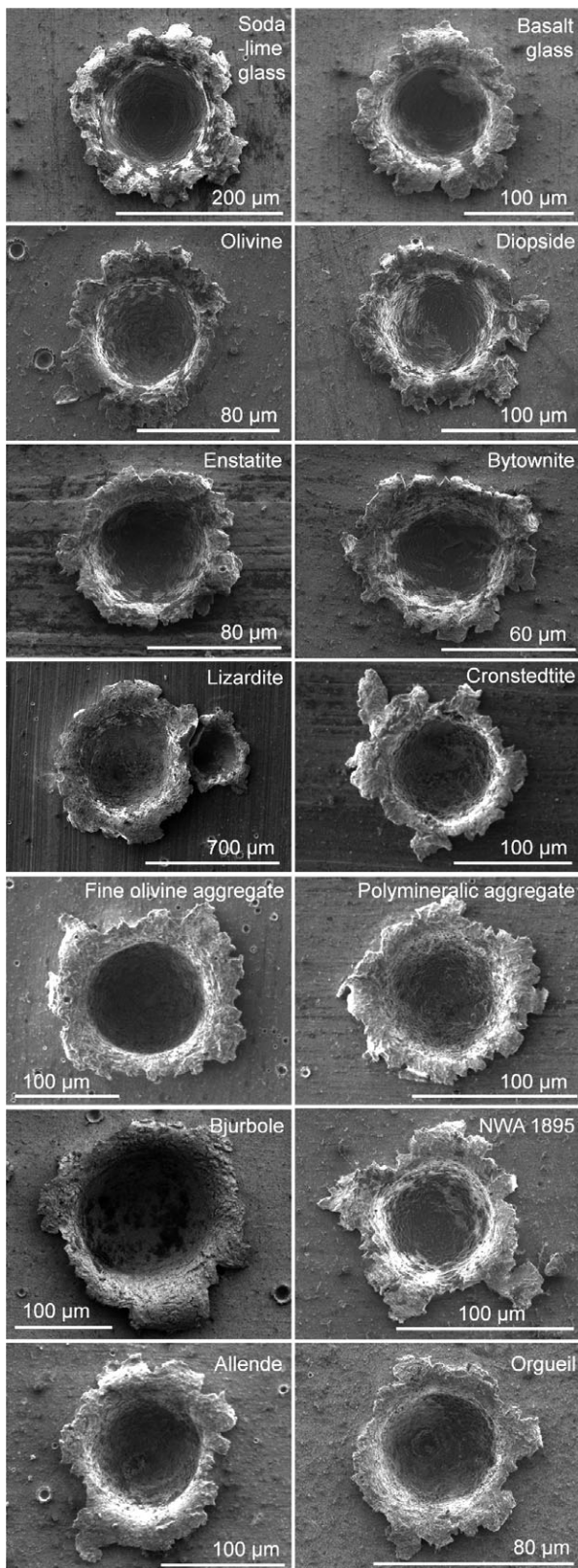


Fig. 4. SEI acquired at low beam energy reveal the wide distribution of impacting particle residue (dark areas) for a variety of impactors.

d) EDX spectra of the crater floor from a range of organic impactors clearly show higher levels of carbon than are found on surrounding areas of alloy. This cannot be attributed to surface contamination from either the experimental process or analytical instrument as the suite of light elements in each case (C, N, and O) are diagnostic of the specific impactor (Fig. 7). The physical structure of the residue is not known, or whether it extends to depth within the frozen metal melt of the crater floor—no FIB analysis or TEM has yet been performed. However, absorption of low-energy X-rays by Al alloy is very efficient, and it is unlikely that a significant light element signal can be collected from beneath even a very thin surface layer. Preliminary studies using time-of-flight secondary ion mass spectrometry (TOF-SIMS) at the University of Manchester (Henkel et al. 2012) have also shown that the surface does yield organic molecular fragments created by impact pyrolysis of the particle. Assuming that all residue was concentrated in a surface layer, we compared the ratio of C:Al X-ray count rates to rates from calibrated known-thickness carbon films, as was used to monitor submicrometer instrument-derived surface contamination during the Stardust Interstellar Preliminary Examination (Stroud et al. 2014). From PMMA we found a residue layer of ~ 12.5 nm, and from PST the thickness was ~ 27 nm. The impactor sizes were again calculated from measured crater dimensions and the polymer impactor size calibration of Kearsley et al. (2007), giving $\sim 2.5\%$ of PMMA retained, and $\sim 2.7\%$ of PST. It should be noted that the detected presence of oxygen in the PMMA residue is not included in the calculation, and probably implies a slightly higher mass of residue retention. However, there is clearly an order of magnitude difference in the quantity of retained material when compared to silicate glass, or silicate-dominated largely crystalline meteorite grains.

Foil Preparation

DEMs showed that the high ductility of the Al 1100 foil allowed $101 \mu\text{m}$ thick Stardust foil to be uplifted by over $200 \mu\text{m}$ without tearing (e.g., Fig. 8). The BEIs (shown as combined stereo anaglyphs in Figs. 9b and 9c) revealed extensive areas of bright impact residue in the craters before preparation. The depth profiles of craters before (Figs. 9a and 9d) and after shape modification (Figs. 9e and 9h) clearly show that craters on Stardust foil can be made much broader and shallower by using the needle technique, bringing all the

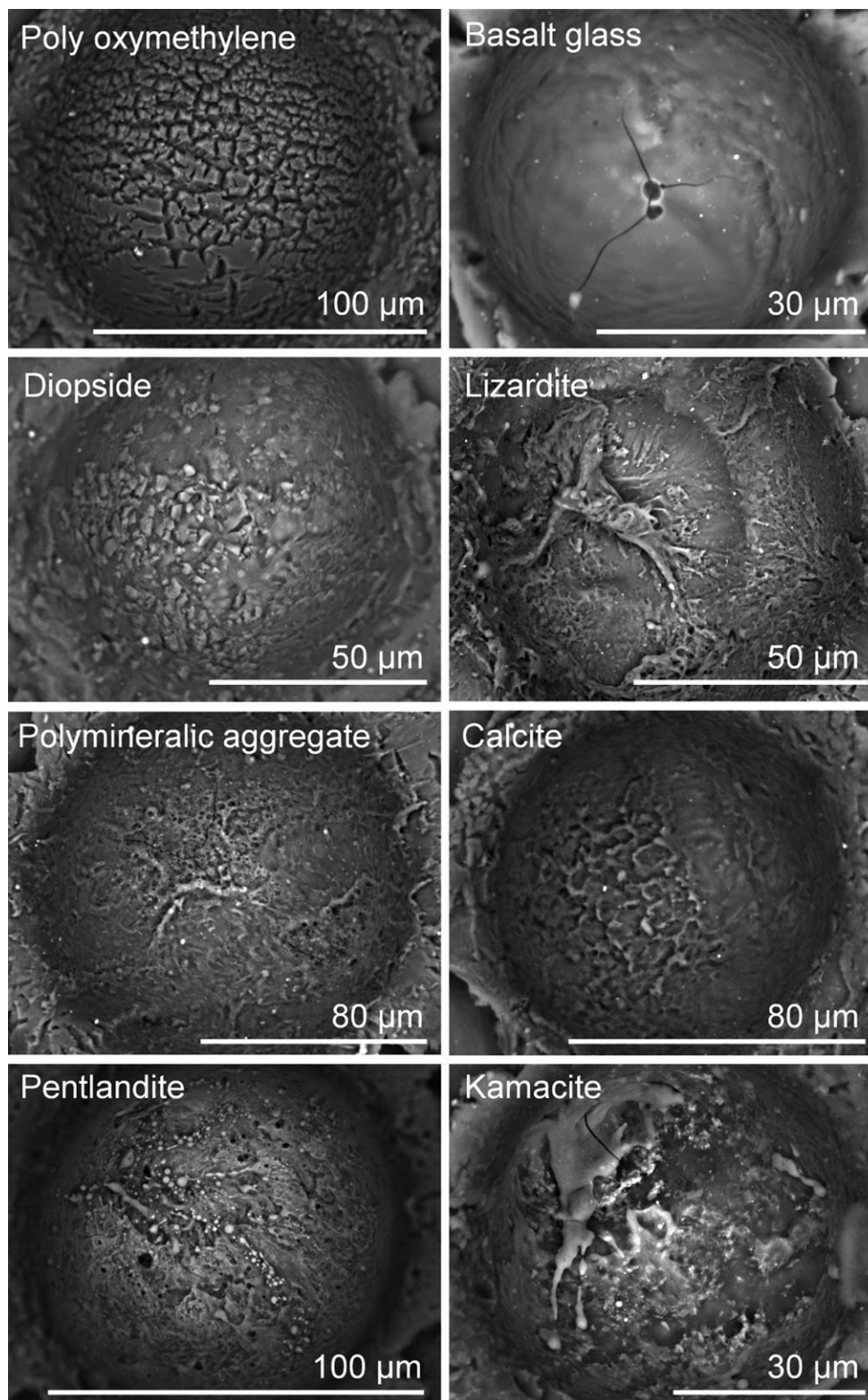


Fig. 5. BEI acquired at high beam energy reveal residue textures from different types of impactor composition and structure.

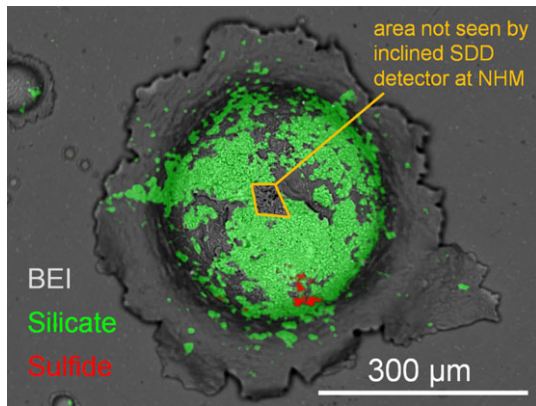


Fig. 6. BEI and superimposed EDX maps show the distribution of silicate and sulfide projectile residue in a crater made by a LGG impact of a grain of Bjurböle ordinary chondrite powder.

residue in the crater to locations suitable for in situ analysis or safe extraction by proven methods.

DISCUSSION

Preliminary examination results (e.g., Kearsley et al. 2008; Leitner et al. 2008; Stadermann et al. 2008) suggested that Wild 2 craters clearly contain valuable material for analysis. Electron images, EDX maps, and FIB sections all demonstrate that for silicate-dominated particles, there is abundant diagnostic particle material retained within Stardust analogue craters of all sizes. Although the accuracy of measurement for impacting particle dimensions and residue thickness in the experiments described above is difficult to assess, the results do indicate that a substantial proportion of silicate grains (~half) is captured by impact onto foil under Stardust encounter conditions (for crater sizes

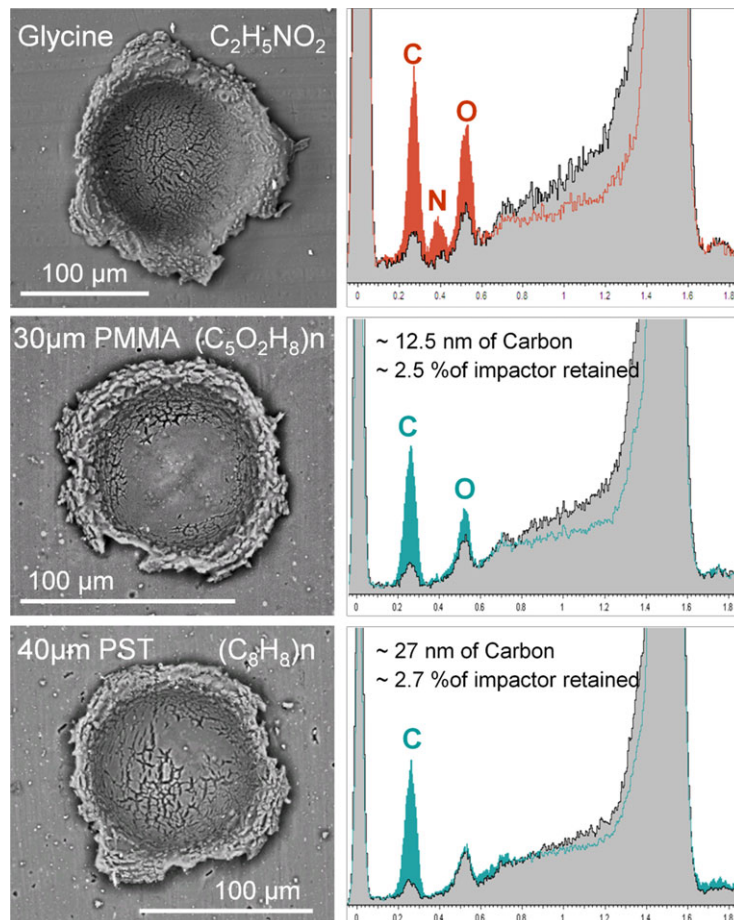


Fig. 7. BEI with associated EDX spectra from craters generated by organic impactors glycine, polymethylmethacrylate (PMMA), and polystyrene (PST). Spectra from residue (orange or blue) are superimposed on background foil (gray), showing distinct signatures for different organic impactors. Residue thickness measured using the protocol of Stroud et al. (2014), and volume calculated from the three-dimensional surface area of the crater (derived from a stereo pair digital elevation model), then compared to impactor volume to assess the proportion retained.

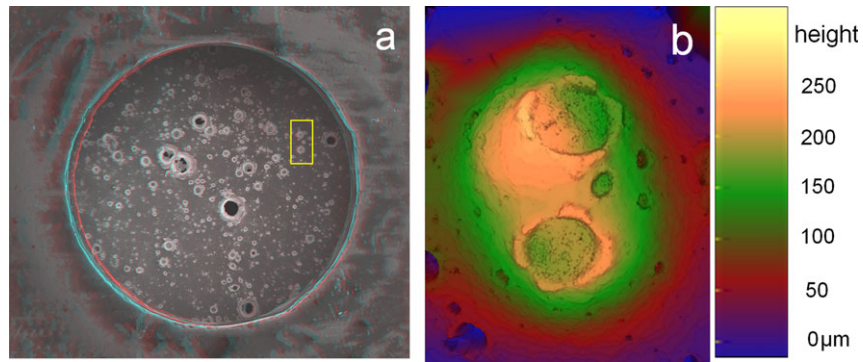


Fig. 8. a) Stereo anaglyph BEI of Stardust foil impacted by galena in LGG shot; the yellow box shows the location of two craters subsequently prepared. b) Digital elevation model of the craters after foil deformation using the steel needle.

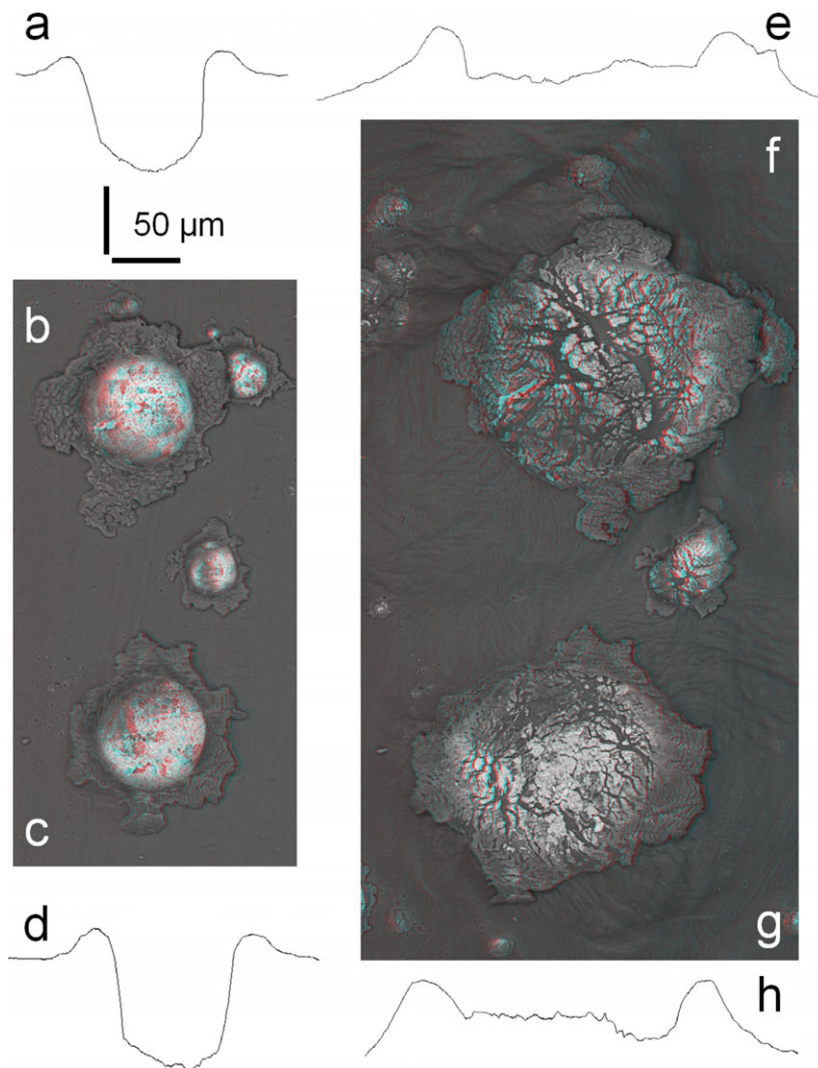


Fig. 9. (a) and (d) Depth profiles; (b) and (c) stereo BEI of two craters before preparation; (e) and (h) depth profiles; (f) and (g) stereo BEI of the same two craters after preparation. Note the greatly reduced depth, increasing the available area for extraction and analysis.

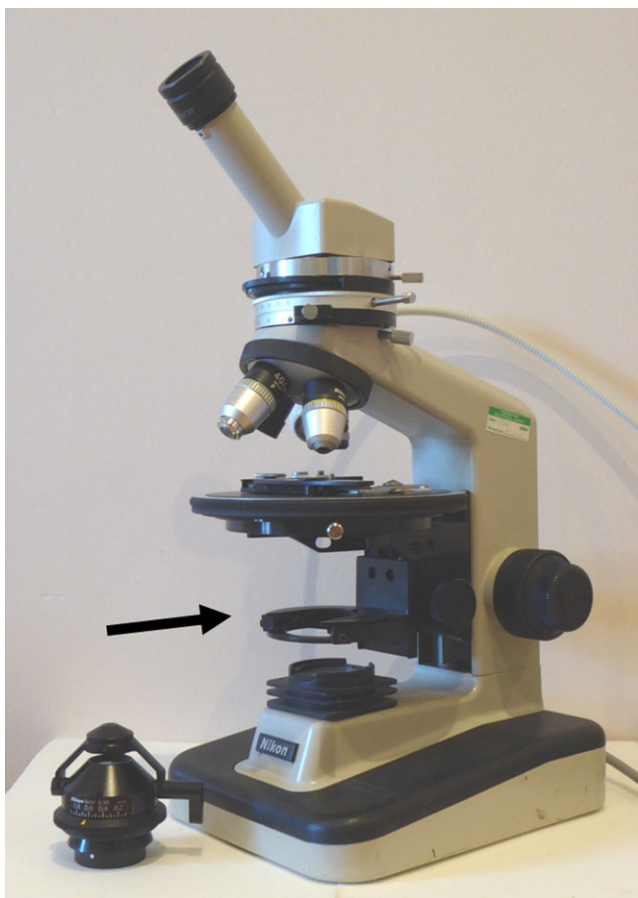


Fig. 10. Microscope, with substage condenser assembly removed, to allow mounting of a needle assembly (at location arrowed) that can be gently raised beneath the stage-clamped foil holder, to deform the foil in a controlled manner.

over the range applicable to Stardust). Our crater data also suggest that much less of the original particle remains for organic impactors, although the light elements observed in each case (C, N, and O) may still be used as a diagnostic of the specific impactor.

Manual deformation of an impacted foil clearly demonstrates that it is straightforward to make the contents of larger Stardust foil craters accessible at or above the level of the preimpact foil surface. The particle remnants can then be analyzed either in situ by diverse techniques (e.g., electron, ion, optical laser, or infrared), or small subsamples can be removed by FIB for further analysis by techniques such as TEM.

This technique could be adapted easily for reliable and reproducible foil preparation by the following method:

1. Prepare an optical microscope by replacing the substage condenser lens with a centered, resin-

mounted vertical needle assembly which can be moved up and down by use of the condenser focus wheel (Fig. 10). The needles are interchangeable, with different sizes available for different sized craters (the needle tip should be approximately equal in diameter to the crater diameter).

2. Place the impacted foil within a holder (a hinge such as Fig. 1, or similar apparatus) that allows access to the foil crater through an aperture from both above and below.
3. Clamp the foil holder into the movable specimen stage of the microscope.
4. Illuminate the foil from above.
5. Center the crater, visible in the holder aperture, to a position below the objective lens, and then focus the microscope onto the surrounding undeformed foil surface.
6. Use slow upward movement of the mounted needle to gradually deform the foil, while the evolving topography is monitored through the microscope. As the base of the crater is brought in line with the preimpact surface, it will come into focus and reshaping of the foil can be halted. The sample is now ready for in situ analysis or the safe removal of small areas of material.

CONCLUSIONS

We demonstrated that it is now possible to safely modify the shape of larger Stardust craters, giving better access to their contents for in situ analysis and the removal of subsamples. We further proposed additional mechanization for highly controlled shape modification. This should prove especially important for the identification and extraction of specific sites of special interest, e.g., presolar grains. In combination with prepreparation EDX mapping (e.g., Wozniakiewicz et al. 2015), and by comparison to data obtained from analogue studies, it will allow both overview and targeted investigation of the preserved mineralogy in larger craters. Given the large volume of material shown here to be retained within silicate-dominated impact craters, this will release another important repository of cometary dust from comet 81P/Wild 2, made available for study by diverse techniques. This may be even more important for organic-rich impactors, where only some 2–3% of the impacting material was found to be retained; making such scarce residues available for analysis is clearly crucial.

Acknowledgments—We thank Fred Hörz of NASA for samples of Stardust foil to use in experiments, STFC for funding the hypervelocity impact facilities and their

staff at the University of Kent, and NHM for access to electron microscopy and microanalysis facilities.

Editorial Handling—Dr. Donald Brownlee

REFERENCES

- Brownlee D., Tsou P., Aléon J., Alexander C. M. O'D., Araki T., Bajt S., Baratta G. A., Bastien R., Bland P., Bleuet P., Borg J., Bradley J. P., Brearley A., Brenker F., Brennan S., Bridges J. C., Browning N., Brucato J. R., Brucato H., Bullock E., Burchell M. J., Busemann H., Butterworth A., Chaussidon M., Chevront A., Chi M., Cintala M. J., Clark B. C., Clemett S. J., Cody G., Colangeli L., Cooper G., Cordier P. G., Daghlian C., Dai Z., D'Hendecourt L., Djouadi Z., Dominguez G., Duxbury T., Dworkin J. P., Ebel D., Economou T. E., Fairey S. A. J., Fallon S., Ferrini G., Ferroir T., Fleckenstein H., Floss C., Flynn G., Franchi I. A., Fries M., Gainsforth Z., Gallien J.-P., Genge M., Gilles M. K., Gillet P., Gilmour J., Glavin D. P., Gounelle M., Grady M. M., Graham G. A., Grant P. G., Green S. F., Grossemy F., Grossman L., Grossman J., Guan Y., Hagiya K., Harvey R., Heck P., Herzog G. F., Hoppe P., Hörz F., Huth J., Hutcheon I. D., Ishii H., Ito M., Jacob D., Jacobsen C., Jacobsen S., Joswiak D., Kearsley A. T., Keller L., Khodja H., Kilcoyne A. L. D., Kissel J., Krot A., Langenhorst F., Lanzirotti A., Le L., Leshin L., Leitner J., Lemelle L., Leroux H., Liu M.-C., Luening K., Lyon I., MacPherson G., Marcus M. A., Marhas K., Matrajt G., Meibom A., Mennella V., Messenger K., Mikouchi T., Mostefaoui S., Nakamura T., Nakano T., Newville M., Nittler L. R., Ohnishi I., Ohsumi K., Okudaira K., Papanastassiou D. A., Palma R., Palumbo M. O., Pepin R. E., Perkins D., Perronnet M., Pianetta P., Rao W., Rietmeijer F., Robert F., Rost D., Rotundi A., Ryan R., Sandford S. A., Schwandt C. S., See T. H., Schlutter D., Sheffield-Parker J. A., Simionovici S., Sitnitsky S. I., Snead C. J., Spencer M. K., Stadermann F. J., Steele A., Stephan T., Stroud R., Susini J., Sutton S. R., Taheri M., Taylor S., Teslich N., Tomeoka K., Tomioka N., Toppani A., Trigo-Rodríguez J. M., Troadec D., Tsuchiyama A., Tuzzolino A. J., Tylliszczak T., Uesugi K., Velbel M., Vellenga J., Vicenzi E., Vincze L., Warren J., Weber I., Weisberg M., Westphal A. J., Wirrick S., Wooden D., Wopenka B., Wozniakiewicz P. A., Wright I., Yabuta H., Yano H., Young E. D., Zare R. N., Zega T., Ziegler K., Zimmerman L., Zinner E., and Zolensky M. 2006. Comet Wild 2 under a microscope. *Science* 314:1711–1716.
- Burchell M. J. and Kearsley A. T. 2009. Short-period Jupiter family comets after Stardust. *Planetary and Space Science* 57:1146–1161.
- Burchell M. J., Cole M. J., McDonnell J. A. M., and Zarnecki J. C. 1999. Hypervelocity impact studies using the 2 MV Van de Graaff dust accelerator and two stage light gas gun of the University of Kent at Canterbury. *Measurement Science & Technology* 10:41–50.
- Burchell M. J., Foster N. J., Kearsley A. T., and Creighton J. A. 2008. Identification of mineral impactors in hypervelocity impact craters in aluminum by Raman spectroscopy of residues. *Meteoritics & Planetary Science* 43:135–142.
- Ebel D. S., Greenberg M., Rivers M. L., and Newville M. 2009. Three-dimensional textural and compositional analysis of particle tracks and fragmentation history in aerogel. *Meteoritics & Planetary Science* 44:1445–1463.
- Flynn G. J., Bleuet P., Borg J., Bradley J. P., Brenker F. E., Brennan S., Bridges J., Brownlee D. E., Bullock E. S., Burghammer M., Clark B. C., Dai Z. R., Daghlian C. P., Djouadi Z., Fakra S., Ferroir T., Floss C., Franchi I. A., Gainsforth Z., Gallien J.-P., Gillet P., Grant P. G., Graham G. A., Green S. F., Grossemy F., Heck P., Herzog G. F., Hoppe P., Hörz F., Huth J., Ignatyev K., Ishii H. A., Janssens K., Joswiak D., Kearsley A. T., Khodja H., Lanzirotti A., Leitner J., Lemelle L., Leroux H., Luening K., MacPherson G. J., Marhas K. K., Marcus M. A., Matrajt G., Nakamura T., Nakamura-Messenger K., Nakano T., Newville M., Papanastassiou D. A., Pianetta P., Rao W., Riekel C., Rietmeijer F. J. M., Rost D., Schwandt C. S., See T. H., Sheffield-Parker J., Simionovici A., Sitnitsky I., Snead C. J., Stadermann F. J., Stephan T., Stroud R. M., Susini J., Suzuki Y., Sutton S. R., Taylor S., Teslich N., Troadec D., Tsou P., Tsuchiyama A., Uesugi K., Vekemans B., Vicenzi E. P., Vincze L., Westphal A. J., Wozniakiewicz P., Zinner E., and Zolensky M. E. 2006. Elemental compositions of Comet 81P/Wild 2 samples collected by Stardust. *Science* 314:1731–1735.
- Foster N. F., Wozniakiewicz P. J., Price M. C., Kearsley A. T., and Burchell M. J. 2013. Identification by Raman spectroscopy of Mg-Fe content of olivine samples after impact at 6 km s⁻¹ onto aluminium foil and aerogel: In the laboratory and in Wild-2 cometary samples. *Geochimica et Cosmochimica Acta* 121:1–14.
- Graham G. A., Teslich N., Dai Z. R., Bradley J. P., Kearsley A. T., and Hörz F. 2006. Focused ion beam recovery of hypervelocity impact residue in experimental craters on metallic foils. *Meteoritics & Planetary Science* 41:159–165.
- Henkel T., Lyon I. C., Kearsley A. T., Price M. C., Cole M. J., and Burchell M. J. 2012. Survival of organic compounds on Al foil under Stardust conditions (abstract #2158). 43rd Lunar and Planetary Science Conference. CD-ROM.
- Hörz F., Bastien R., Borg J., Bradley J. P., Bridges J. C., Brownlee D. E., Burchell M. J., Cintala M. J., Dai Z. R., Djouadi Z., Dominguez G., Economou T. E., Fairey S. A. J., Floss C., Franchi I. A., Graham G. A., Green S. F., Heck H., Hoppe P., Huth J., Ishii H., Kearsley A. T., Kissel J., Leitner J., Leroux H., Marhas M., Messenger K., Schwandt C. S., See T. H., Snead S., Stadermann F. J., Stephan T., Stroud R., Teslich N., Trigo-Rodríguez J. M., Tuzzolino A. J., Troadec D., Tsou P., Warren J., Westphal A., Wozniakiewicz P. J., Wright I., and Zinner E. 2006. Impact features on Stardust: Implications for comet 81P/Wild 2 dust. *Science* 314:1716–1719.
- Ishii H. A. and Bradley J. P. 2006. Macroscopic subdivision of silica aerogel collectors for sample return missions. *Meteoritics & Planetary Science* 41:233–236.
- Ishii H. A. and Bradley J. P. 2015. Transmission electron microscopy advances reveal subtle comet dust differences. 78th Annual Meeting of the Meteoritical Society. *Meteoritics & Planetary Science* 50(S1):A181.
- Ishii H. A., Graham G. A., Kearsley A. T., Grant P. G., Snead C. J., and Bradley J. P. 2005. Rapid extraction of dust impact tracks from silica aerogel by ultrasonic microblades. *Meteoritics & Planetary Science* 40:1741–1747.
- Kearsley A. T., Graham G. A., Burchell M. J., Cole M. J., Dai Z. R., Teslich N., Bradley J. P., Chater R.,

- Wozniakiewicz P. A., Spratt J., and Jones G. 2007. Analytical scanning and transmission electron microscopy of laboratory impacts on Stardust aluminum foils: Interpreting impact crater morphology and the composition of impact residues. *Meteoritics & Planetary Science* 42:191–210.
- Kearsley A. T., Borg J., Graham G. A., Burchell M. J., Cole M. J., Leroux H., Bridges J. C., Hörz F., Wozniakiewicz P. J., Bland P. A., Bradley J. P., Dai Z. R., Teslich N., See T., Hoppe P., Heck P. R., Huth J., Stadermann F. J., Floss C., Marhas K., Stephan T., and Leitner J. 2008. Dust from comet Wild 2: Interpreting particle size, shape, structure and composition from impact features on the Stardust aluminum foils. *Meteoritics & Planetary Science* 43:41–73.
- Kobayashi T., Sekine T., Fatyanov O. V., Takazawa E., and Zhu Q. Y. 1998. Radioactive temperature of soda lime glass in its shocked compressed state. *Journal of Applied Physics* 83:1711–1716.
- Leitner J., Stephan T., Kearsley A. T., Hörz F., Flynn G. J., and Sandford S. A. 2008. TOF-SIMS analysis of crater residues from Wild 2 cometary particles on Stardust Aluminum foil. *Meteoritics & Planetary Science* 43:161–186.
- Leroux H., Rietmeijer F. J. M., Velbel M. A., Brearley A. J., Jacob D., Langenhorst F., Bridges J. C., Zega T. J., Stroud R. M., Cordier P., Harvey R. P., Lee M., Gounelle M., and Zolensky M. E. 2008a. A TEM study of thermally modified comet 81P/Wild 2 dust particles by interactions with the aerogel matrix during the Stardust capture process. *Meteoritics & Planetary Science* 43:97–120.
- Leroux H., Stroud R. M., Dai Z. R., Graham G. A., Troadec D., Bradley J. P., Teslich N., Borg J., Kearsley A. T., and Hörz F. 2008b. Transmission electron microscopy of cometary residues from micron-sized craters in the Stardust Al foils. *Meteoritics & Planetary Science* 43:143–160.
- Marsh S. P. 1980. *LASL shock Hugoniot data*. Los Angeles: The University of California Press. 674 p.
- Melosh H. J. 1989. *Impact cratering: A geologic process*. Oxford: Oxford University Press.
- Nakamura T., Noguchi T., Tsuchiyama A., Ushikubo T., Kita N. T., Valley J. W., Zolensky M. E., Kakazu Y., Sakamoto K., Mashio E., Uesugi K., and Nakano T. 2008. Chondrule like objects in short-period comet 81P/Wild 2. *Science* 321:1664–1667.
- Nakamura-Messenger K., Keller L. P., Clemett S. J., Messenger S., and Ito M. 2011. Nanometer-scale anatomy of entire Stardust tracks. *Meteoritics & Planetary Science* 46:1033–1051.
- Price M. C., Kearsley A. T., Burchell M. J., Hörz F., Borg J., Bridges J. C., Cole M. J., Floss C., Graham G., Green S. F., Hoppe P., Leroux H., Marhas K. K., Park N., Stroud R., Stadermann F. J., Teslich N., and Wozniakiewicz P. J. 2010. Comet 81P/Wild 2: The size distribution of finer (sub 10-micrometre) dust collected by the Stardust spacecraft. *Meteoritics & Planetary Science* 45:1409–1428.
- Snead C. J. 2016. Ion probe measurements of comet dust: Investigating oxygen isotope heterogeneity in the solar system. Ph.D. thesis, University of California, Los Angeles, California, USA.
- Snead C. J., McKeegan K. D., and Boehnke P. 2014. Oxygen isotope compositions of two stardust impact crater residues (abstract #2928). 45th Lunar and Planetary Science Conference. CD-ROM.
- Snead C. J., McKeegan K. D., Keller L. P., and Messenger S. 2017. Ion microprobe measurements of comet dust and implications for models of oxygen isotope heterogeneity in the solar system (abstract #2623). 48th Lunar and Planetary Science Conference. CD-ROM.
- Stadermann F. J. and Floss C. 2008. Determining the elemental and isotopic makeup of cosmic dust from residues in impact craters: Preparation for the ISPE (abstract #5105). *Meteoritics & Planetary Science* 43:A147.
- Stadermann F. J., Hoppe P., Floss C., Heck P. R., Hörz F., Huth J., Kearsley A. T., Leitner J., Marhas K. K., McKeegan K. D., and Stephan T. 2008. Stardust in STARDUST—The C, N, and O isotopic compositions of Wild 2 cometary matter in Al foil impacts. *Meteoritics & Planetary Science* 43:299–314.
- Stodolna J., Jacob D., and Leroux H. 2009. A TEM study of four particles extracted from the Stardust track 80. *Meteoritics & Planetary Science* 44:1511–1518.
- Stroud R. M., Allen C., Ansari A., Anderson D., Bajt S., Bassim N., Bastien R. S., Bechtel H. A., Borg J., Brenker F. E., Bridges J., Brownlee D. E., Burchell M., Burghammer M., Butterworth A. L., Changela H., Cloetens P., Davis A. M., Doll R., Floss C., Flynn C. G., Frank D. R., Gainsforth Z., Grün E., Heck P. R., Hillier J. K., Hoppe P., Huth J., Hvide B., Kearsley A., King A. J., Kotula P., Lai B., Leitner J., Lemelle L., Leroux H., Leonard A., Lettieri R., Marchant W., Nittler L. R., Oglione R., Ong W. J., Postberg F., Price M. C., Sandford S. A., Tresseras J.-A. S., Schmitz S., Schoonjans T., Schreiber K., Silversmit G., Simionovici A. S., Solé V. A., Srama R., Stephan T., Sterken V. J., Stodolna J., Sutton S., Trieloff M., Tsou P., Tsuchiyama A., Tyliczszak T., Vekemans B., Vincze L., Westphal A. J., Von Korff J., Zevin D., and Zolensky M. E. 2014. Stardust interstellar preliminary examination XI: Identification and elemental analysis of impact craters on Al foils from the Stardust Interstellar Dust Collector. *Meteoritics & Planetary Science* 49:1698–1719.
- Tsuchiyama A., Nakamura T., Okazaki T., Uesugi K., and Nakano T. 2009. Three-dimensional structures and elemental distributions of Stardust impact tracks using synchrotron microtomography and X-ray fluorescence analysis. *Meteoritics & Planetary Science* 44:1203–1224.
- Westphal A. J., Snead C., Butterworth A., Graham G. A., Bradley J. P., Bajt S., Grant P. G., Bench G., Brennan S., and Pianetta P. 2004. Aerogel keystones: Extraction of complete hypervelocity impact events from aerogel collectors. *Meteoritics & Planetary Science* 39:1375–1386.
- Westphal A. J., Bridges J. C., Brownlee D. E., Butterworth A. L., DeGregorio B. T., Dominguez G., Flynn G. J., Gainsforth Z., Ishii H. A., Joswiak D., Nittler L. R., Oglione R. C., Palma R., Pepin R. O., Stephan T., and Zolensky M. E. 2017. The future of Stardust science. *Meteoritics & Planetary Science* 52:1859–1898.
- Wozniakiewicz P. J., Kearsley A. T., Burchell M. J., Foster N. J., Cole M. J., Bland P. A., and Russell S. A. R. 2009. Analysis of residues resulting from laboratory impacts into aluminum 1100 foil: Implications for Stardust crater analyses. *Meteoritics & Planetary Science* 44:1541–1559.
- Wozniakiewicz P. J., Ishii H. A., Kearsley A. T., Burchell M. J., Bland P. A., Bradley J. P., Dai Z., Teslich N., Collins G. S., Cole M. J., and Russell S. S. 2011. Investigation of iron sulfide impact crater residues: A combined analysis by scanning and transmission electron microscopy. *Meteoritics & Planetary Science* 46:1007–1024.

- Wozniakiewicz P. J., Ishii H. A., Kearsley A. T., Burchell M. J., Bradley J. P., Price M. C., Teslich N., Lee M. R., and Cole M. J. 2012a. Stardust impact analogues: Resolving pre- and post-impact mineralogy in Stardust Al foils. *Meteoritics & Planetary Science* 47:708–728.
- Wozniakiewicz P. J., Kearsley A. T., Ishii H. A., Burchell M. J., Bradley J. P., Teslich N., Cole M. J., and Price M. C. 2012b. The origin of crystalline residues in Stardust Al foils: Surviving cometary dust or crystallized impact melts? *Meteoritics & Planetary Science* 47:660–670.
- Wozniakiewicz P. J., Ishii H. A., Kearsley A. T., Bradley J. P., Price M. C., Burchell M. J., Teslich N., and Cole M. J. 2015. The survivability of phyllosilicates and carbonates impacting Stardust Al foils: Facilitating the search for cometary water. *Meteoritics & Planetary Science* 50:2003–2023.
- Zolensky M., Nakamura-Messenger K., Rietmeijer F., Leroux H., Mikouchi T., Ohsumi K., Simon S., Grossman L., Stephan T., Weisberg M., Velbel M., Zega T., Stroud R., Tomeoka K., Ohnishi I., Tomioka N., Nakamura T., Matrajt G., Joswiak D., Brownlee D., Langenhorst F., Krot A., Kearsley A., Ishii H., Graham G., Dai Z. R., Chi M., Bradley J., Hagiya K., Gounelle M., Keller L., and Bridges J. 2008. Comparing Wild 2 particles to chondrites and IDPs. *Meteoritics & Planetary Science* 43:261–272.
-